ELSEVIER

Journal of Structural Geology 26 (2004) 2203–2209

JOURNAL OF STRUCTURAL GEOLOGY

www.elsevier.com/locate/jsg

Triaxial stress state deep in orogenic belts: an example from Turkey

T. Masuda*, S. Nakayama, N. Kimura, K. Onodera, A. Okamoto

Institute of Geosciences, Shizuoka University, Shizuoka 422-8529, Japan

Received 20 October 2003; received in revised form 25 May 2004; accepted 4 June 2004
Available online 19 August 2004

Abstract

A rare metachert pebble containing amphibole grains with microboudin structures in a wide range of orientations provides an opportunity to perform stress analysis in two orthogonal orientations on the foliation surface. The sample was analysed by the microboudin method to infer the triaxial stress state during microboudinage. Stress parameters proportional to the far-field differential stress were determined for sodic amphibole grains in the two orientations. The ratio of the stresses in the two orthogonal orientations $(\sigma_1-\sigma_2)/(\sigma_1-\sigma_3)$ was calculated to be 0.64, indicating that σ_2 lies closer to the midpoint between σ_1 and σ_3 than to σ_3.

Keywords: Triaxial stress state; Microboudinage; Sodic amphibole; Quartz matrix; Turkey

1. Introduction

The triaxial stress state deep in orogenic belts is a major factor in the study of plastic deformation of metamorphic tectonites as stress drives rock deformation, mountain building and plate tectonics. A number of palaeopiezometers have been proposed to estimate the palaeo-differential stress $(\sigma_1-\sigma_3)$ (e.g. Jamison and Spang, 1976; Mercier et al., 1977; Twiss, 1986; Passchier and Trouw, 1996), and many of the techniques have been applied to estimating palaeo-stress for rocks in shear zones and other geological conditions (e.g. Weathers et al., 1979; Etheridge and Wilkie, 1981; Ord and Christie, 1984; Rowe and Rutter, 1990; Lacombe, 2001). However, there as yet has been no quantitative analysis of σ_2 with respect to σ_1 and σ_3.

Although the importance of specifying the triaxial stress state in orogenic belts is not always clear in two-dimensional mechanical analyses, advanced studies using three-dimensional configurations require σ_2 in addition to σ_1 and σ_3 as a boundary condition for simulation. Thus, dealing with σ_2 is indispensable for the comprehensive understanding of mountain-building processes in orogenic belts. The present paper applies the microboudin method (Masuda et al., 2003, 2004) for the palaeo-stress analysis of a rare metachert sample collected from Turkey and estimates σ_2 with respect to σ_1 and σ_3 for this sample.

2. Sample

The metachert pebble was collected from a small gully near Eskisehir, central Turkey (Fig. 1). This area is part of a Cretaceous high-pressure metamorphic belt, which formed on the northern margin of the Tethys during its convergence (e.g. Okay et al., 1998; Okay, 2002). Okay (2002) estimated the peak metamorphic conditions to be 430 °C and 2.4 GPa for this region. The metachert consists mainly of quartz, with subordinate sodic amphibole, tourmaline, epidote, garnet and muscovite, and exhibits a clear foliation defined by parallel alignment of muscovite and banding of different coloured layers. No folding is apparent in the sample.

On the foliation surface under an optical microscope, columnar sodic amphibole and tourmaline grains can be seen arranged in various orientations (Fig. 2), and the orientation of the mineral lineation is difficult to determine by simple observation. This sample is rare as it displays long axes of sodic amphibole grains and microboudin structures in a wide range of orientations.

* Corresponding author. Fax: +81-54-238-0491
E-mail address: setmasu@ipc.shizuoka.ac.jp (T. Masuda).

0191-8141/$ - see front matter © 2004 Elsevier Ltd. All rights reserved.
doi:10.1016/j.jsg.2004.06.005

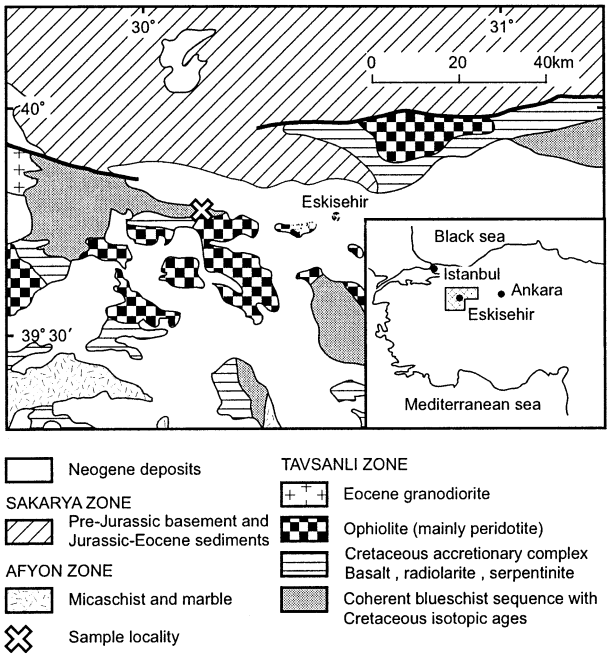

Fig. 1. Geological map of the Eskisehir area modified after Okay (2002). The metachert sample came from the Tavsanli zone.

3. Lineation

Shape-preferred orientation of sodic amphibole on the foliation surface was determined by the statistical method proposed by Masuda et al. (1999). The angle (θ_i) between the long axis of the ith sodic amphibole grain and an arbitrarily drawn base line was measured, and a von Mises distribution was applied to the results (Fig. 3) to determine the mean orientation ($\bar{\theta}$), the confidence interval (d_0) and the concentration parameter (κ). The lineation is then taken as the orientation of $\bar{\theta}$. The obtained value of κ was 0.8.

4. Microboudinage structures

Two groups of sodic amphibole grains (p- and c-groups) were defined on the foliation surface: p-group grains were defined as having long axes oriented parallel to the lineation ($\pm 15°$), and c-group grains were defined as having long axes oriented perpendicular to the lineation ($\pm 15°$). The p-group grains were fractured perpendicular to the long axis of the grain and pulled apart parallel to the lineation, while the c-group grains were fractured perpendicular to the long axis and pulled apart perpendicular to the lineation. Sodic amphibole grains in other orientations were also fractured perpendicular to the long axis and pulled apart parallel to their long axis. Such occurrences imply that microboudins did not undergo remarkable rotation during or after microboudinage, suggesting that microboudinage proceeded in a coaxial strain field on the foliation surface, and that the strain on the surface is extensional in all directions.

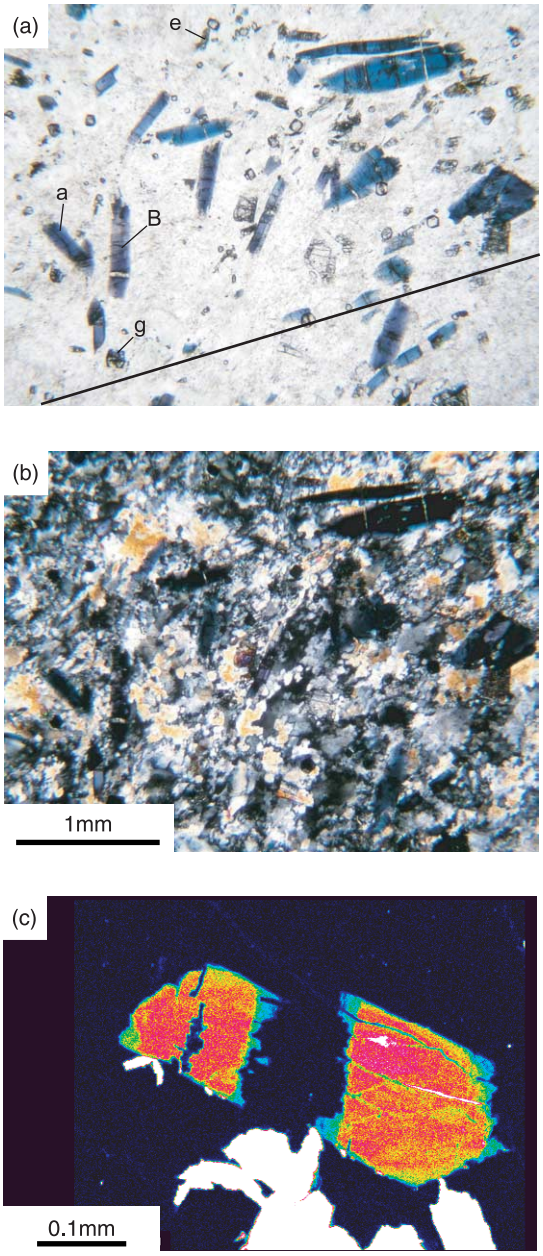

Fig. 2. Photomicrographs of the metachert cut parallel to the foliation. (a) Open nicols. (b) Crossed nicols. Black line in (a) indicates the orientation of $\bar{\theta}$ which is regarded as the orientation of the lineation. a = sodic amphibole, e = epidote, g = garnet, B = boudinaged sodic amphibole. (c) An example of Al zoning pattern of amphibole boudins revealed with an EPMA at the University of Tokyo (JEOL 8900). The host amphibole is glaucophane and the overgrown amphibole in the interboudin gap is magnesioriebeckite. Increase in Al content is exhibited by blueish to reddish colours. Mineral in black = quartz, mineral in white = muscovite.

As none of the microboudins appear to be pinched at the edges (Fig. 2), the competence contrast between sodic amphibole and quartz is considered to be very high at the time of fracturing and subsequent pull-apart (e.g. Ramsay, 1967). Overgrowth of amphibole sometimes occurs on the fracture planes in the interboudin gaps (cf. Misch, 1969). An EPMA analysis revealed that the host amphibole is mostly

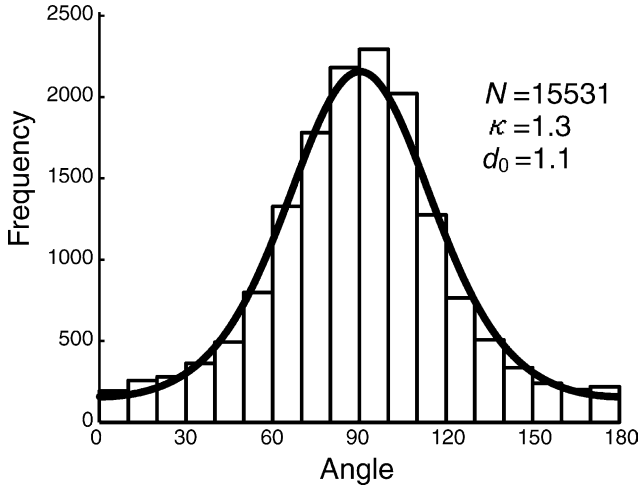

Fig. 3. Frequency distribution of orientation angles and a fitting curve for the von Mises distribution. The distribution is arranged to set $\bar{\theta} = 90°$. κ is the concentration parameter, d_0 is the confidence interval for the critical region of 0.05, and N is the total number of measured sodic amphibole grains.

glaucophane and the overgrown one in the interboudin gaps is magnesioriebeckite (Fig. 2c). Observation of thin sections cut parallel to the lineation and perpendicular to the foliation revealed that the long axes of sodic amphibole grains are largely oriented parallel to the foliation.

5. Measurement of sodic amphibole grains

The widths, lengths and interboudin-gap distances of microboudinaged grains, and the widths and lengths of intact grains were measured (Fig. 4). The overgrown magnesioriebeckite was ignored from the measurement. The distribution of widths and aspect ratios before microboudinage is shown in Fig. 5. The p- and c-group grains show similar widths, demonstrating that the size effect of the fracture strength of sodic amphibole grains can be ignored.

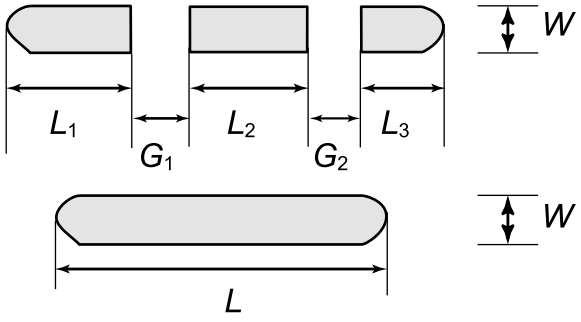

Fig. 4. Grain size of microboudinaged grains (top) and intact grains (bottom). The aspect ratio is calculated as $r = L/W$ (L = length, W = width). L in the top grain is calculated as $L = \Sigma L_i$. L_i and G_i are used to restore the history of microboudinage by the strain reversal method (Ferguson, 1981; Lloyd and Condliffe, 2003).

6. Strain analysis

The strain reversal method (Ferguson, 1981; Lloyd and Condliffe, 2003) provides the natural-log strain of microboudinage after fracturing. Strain accumulation is recorded by an increase in the interboudin-gap distance, and the record begins in the instant of fracturing. The interboudin-gap distance then increases with increasing rock strain until the quartz matrix ceases to deform plastically. At this point, the microboudin structures are frozen. Fig. 6 shows schematically how the microboudinage history can be reconstructed by the strain reversal method.

The timing of fracturing varies from boudin to boudin as revealed by the differences of accumulated strains reflected in the variable interboudin-gap distances. In contrast, the time at which all the microboudinage structures ceased to separate due to cessation of the plastic deformation of quartz is considered to be synchronous, because the brittle–plastic transition temperature is considered to be common for all the quartz grains. Thus, the cessation of plastic deformation is considered as a marker of the end of the history of microboudinage. Therefore, the cessation temperature of plastic deformation of quartz (T_0) and the time at which microboudinage was frozen (t_0) is specified as shown in Fig. 7. Inverse natural strain ε_{inv} is taken by adjusting the time of zero-strain to t_0. Inverse natural strain is scaled back to the past, and is given as a negative value.

Fig. 8 shows the relationship between the aspect ratio of sodic amphibole at the fracturing (ordinate) and ε_{inv} (abscissa) for the fracturing. No systematic change in aspect ratio can be seen with increasing ε_{inv}. Fig. 9 shows the frequency distributions of fractures with respect to aspect ratio. The frequency distribution exhibits a clear peak at $\varepsilon_{inv} = -0.05$ and -0.04 for the p- and c-group grains, respectively. Frequencies are non-zero at $\varepsilon_{inv} = -0.01$ for the two groups, indicating that new fractures formed immediately prior to the cessation of plastic flow of quartz at $t = t_0$ (Fig. 7). As the new fractures are considered to be the result of increasing differential stress, so the differential stress is considered to have been increased up to $t = t_0$, after which there is no record of stress history.

The proportion of broken grains is defined as the ratio of the number of broken grains relative to the total (broken + intact) grains. The proportion with respect to the aspect ratio is the most fundamental parameter in the stress analysis performed later. All grains that ever existed during the history of microboudinage are considered. The frequency distributions of boudinaged and intact grains with respect to aspect ratio are shown in Fig. 10; and the proportion of boudinaged grains is plotted in Fig. 11. These data correspond to microboudin data at $t = t_0$.

7. Stress analysis

Stress analysis was performed using the refined

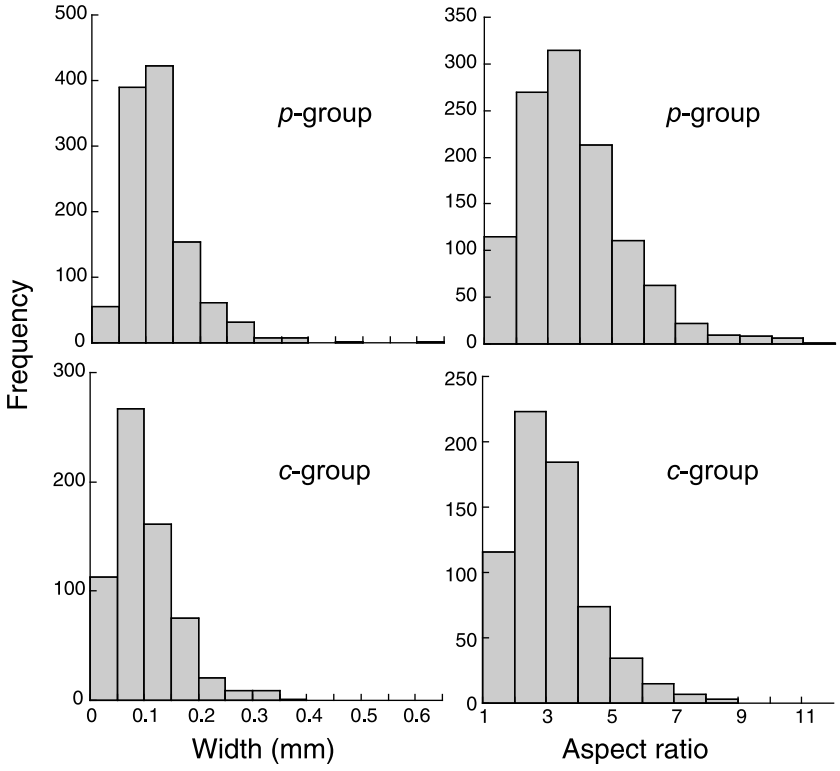

Fig. 5. Frequency distribution of the width (left) and aspect ratio (right) of p- and c-group sodic amphibole grains before microboudinage.

microboudin method of Masuda et al. (2003, 2004). The design of the original microboudin method (Masuda et al., 1989, 1990) was motivated by a series of studies by Ferguson and Lloyd (e.g. Ferguson, 1981; Lloyd et al., 1982), and the refinement (Masuda et al., 2003, 2004) was suggested by the studies of Ji and co-workers (Ji and Zhao, 1993; Zhao and Ji, 1997; Ji and Saruwatari, 1998; Ji et al., 1998). The method assumes mid-point fracturing of fibres (Masuda and Kuriyama, 1988) and mechanically welded interfaces between the fibre and the matrix. These assumptions seem to be valid for fibres with aspect ratio of <20 (Masuda et al., 2004). Although the method does not provide the absolute magnitude of differential stress, it does provide a relative magnitude that is sufficient to specify the triaxial stress state.

Fracturing of columnar mineral grains is a statistical phenomenon and is assumed to be well-described by the Weibull probability density function (e.g. Weibull, 1939; Epstein, 1948). The theoretically predicted proportion of boudinaged grains is consequently given by $G(r, \lambda)$, which is a function of aspect ratio (r) and the stress parameter (λ)

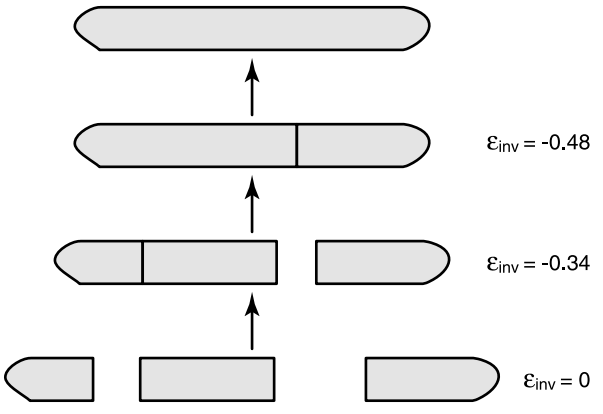

Fig. 6. Scheme of progressive microboudinage with increasing strain. After microboudinage there are two fractured grains and three intact grains. Inverse natural strain (ε_{inv}) is indicated for each stage.

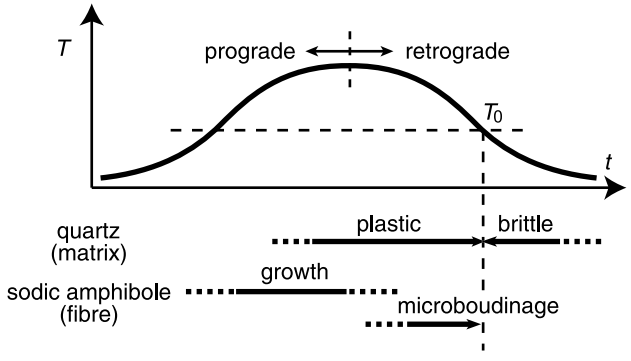

Fig. 7. Scheme of microboudinage stage in the metamorphic history. T_0 is the brittle–plastic transition temperature above which quartz deforms plastically, and t_0 is the marker time at which temperature reached T_0 in the retrograde stage. This figure indicates that the temperature range at which microboudinage occurred is not directly related to the peak temperature in the rock.

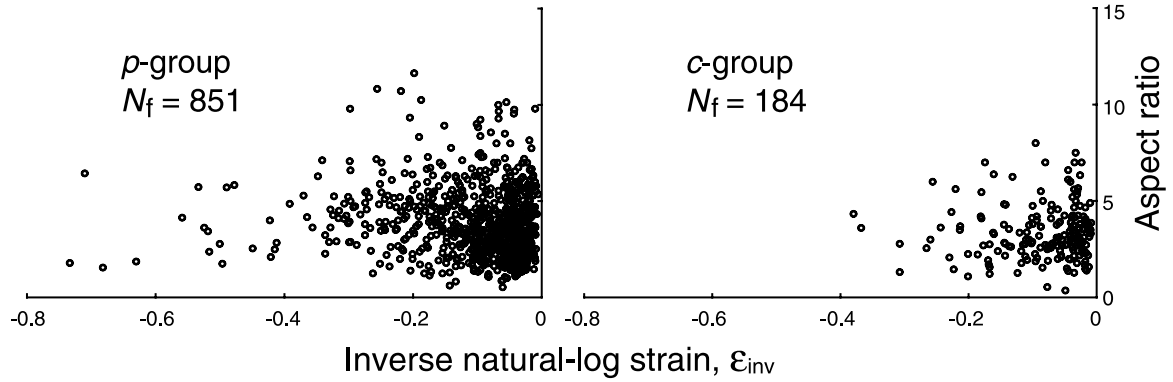

Fig. 8. Aspect ratio and inverse natural strain (ε_{inv}) at fracturing for p- and c-group sodic amphibole grains. N_f is the number of fractured grains.

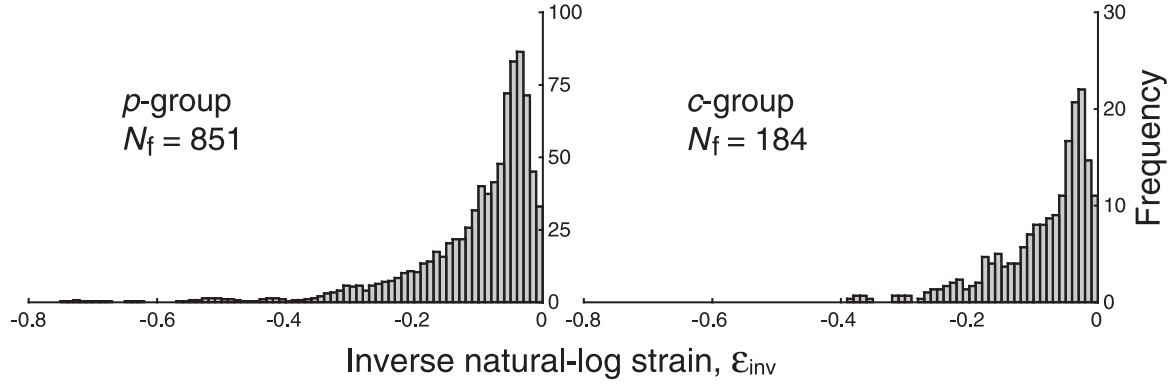

Fig. 9. Frequency distribution of fractures with respect to inverse natural strain (ε_{inv}) for p- and c-group sodic amphibole grains. N_f is the number of fractured grains.

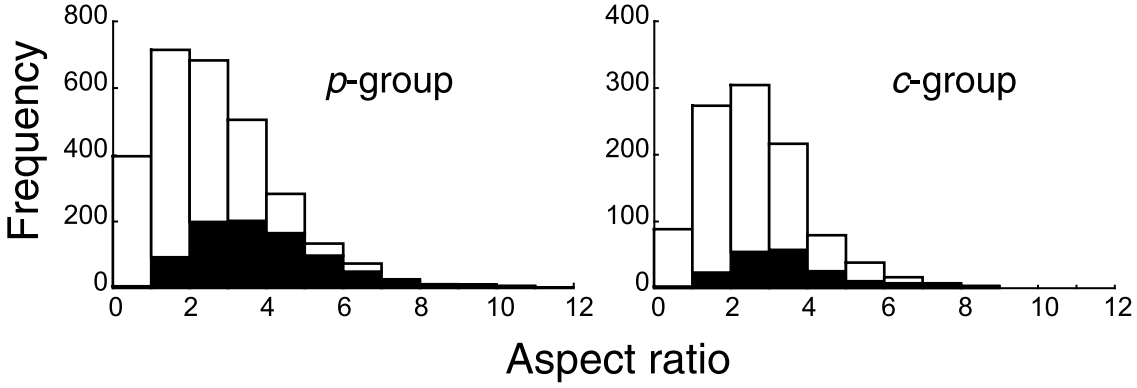

Fig. 10. Frequency distribution of boudinaged (in black) and intact grains (in white) with respect to aspect ratio for p- and c-group sodic amphibole grains.

defined as

$$G(r,\ \lambda) = 1 - \exp\left[-\frac{m-1}{m} r\lambda^m \left(\frac{E_f}{E_q}\right)^m - \left\{1 - \left(1 - \frac{E_q}{E_f}\right)\frac{1}{\cosh(A_0 r)}\right\}^m\right] \quad (1)$$

where m is the Weibull modulus, E_f and E_q are the elastic constants of the fibre material and the matrix, and A_0 is a constant (for derivation of Eq. (1) see Masuda et al. (2003)). The constants E_f/E_q and A_0 for the sodic amphibole fibre and quartz matrix are 1.2 and 0.5, respectively. The data book by Simmons and Wang (1971) was consulted to obtain these values. The stress parameter λ is defined as

$$\lambda = \frac{\sigma_0}{S^*} \quad (2)$$

where σ_0 is the far-field differential stress and S^* is the modal fracture strength of sodic amphibole at $r=1$. As the Weibull modulus is unknown at present, m is regarded as a variable and the probability density function $G(r, \lambda)$ is replaced by $G(r, m, \lambda)$, which can then be compared with the measured proportion of microboudinaged grains $M(r)$ (Fig. 11). The

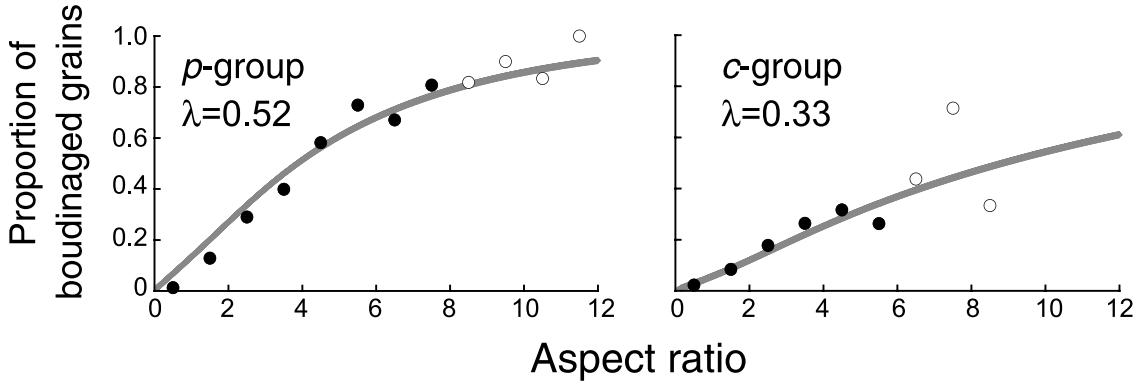

Fig. 11. Proportion of boudinaged grains with respect to aspect ratio at $\varepsilon_{inv}=0$. Solid and open circles indicate reliable and unreliable data (>25 measured grains are regarded as reliable). The curve represents the best-fit $G(r, m, \lambda)$ using reliable data. The value of λ for each group is indicated.

sum of the square difference between $M(r)$ and $G(r, m, \lambda)$ as a function of m and λ is defined as

$$T(m, \lambda) = \sum_r [G(r, m, \lambda) - M(r)] \quad (3)$$

The values of m and λ are then determined to minimize $T(m, \lambda)$.

Stress analysis of the Eskisehir metachert was performed separately for the p- and c-groups of sodic amphibole grains, and the following two relationships were defined for each group:

$$\lambda_p = \frac{\sigma_p}{S^*} \quad (4)$$

and

$$\lambda_c = \frac{\sigma_c}{S^*} \quad (5)$$

where λ_p and λ_c are the stress parameters for the p- and c-groups, and σ_p and σ_c are the far-field differential stresses contributing to the microboudinage of the p- and c-group grains, respectively. The S^* value is common for the two equations but currently unknown and, as a consequence, σ_p and σ_c were not determined in this study. The analysis gave $\lambda_p=0.52$, $\lambda_c=0.33$ and $m=2$. The obtained value of m is realistic when compared with the Weibull modulus of other ceramic materials (e.g. Petry et al., 1997).

As λ_p is larger than λ_c and the strain field is considered to be coaxial, the far-field differential stresses σ_p and σ_c can presumably be expressed as follows.

$$\sigma_p = \sigma_1 - \sigma_3 \quad (6)$$

$$\sigma_c = \sigma_1 - \sigma_2 \quad (7)$$

where σ_1, σ_2 and σ_3 are the principal stresses ($\sigma_1>\sigma_2>\sigma_3$). The triaxial stress state is well represented by the ratio of $\sigma_1-\sigma_2$ to $\sigma_1-\sigma_3$. The ratio ranges from 0 to 1: when $(\sigma_1-\sigma_2)/(\sigma_1-\sigma_3)=0$, $\sigma_1=\sigma_2$; and when $(\sigma_1-\sigma_2)/(\sigma_1-\sigma_3)=1$, $\sigma_2=\sigma_3$. When $(\sigma_1-\sigma_2)/(\sigma_1-\sigma_3)=0.5$, σ_2 is exactly at the midpoint between σ_1 and σ_3. Eqs. (4)–(7) lead to the following expression:

$$\frac{\sigma_1-\sigma_2}{\sigma_1-\sigma_3} = \frac{\sigma_c}{\sigma_p} = \frac{S^*\lambda_c}{S^*\lambda_p} = \frac{\lambda_c}{\lambda_p}. \quad (8)$$

Eq. (8) allows the ratio to be calculated from λ_p and λ_c. As $\lambda_p=0.52$ and $\lambda_c=0.33$ for the Eskisehir metachert, the ratio is 0.64, indicating that σ_2 lies close to the midpoint between σ_1 and σ_3 than to σ_3. As estimated, λ_p and λ_c are only relevant at $t=t_0$ when $T=T_0$ (Fig. 7) and the ratio is also relevant only at $t=t_0$.

Acknowledgements

The authors thank Mevlana C. Baykul and his family for help in Eskisehir, Hideki Mori for preparing thin sections, Shaocheng Ji and A.I. Okay for constructive comments, and Joao Hippertt for kind editing. This study was financially supported by the Japan Society for the Promotion of Science.

References

Epstein, B., 1948. Statistical aspects of fracture problems. Journal of Applied Physics 19, 140–147.

Etheridge, M.A., Wilkie, J.C., 1981. An assessment of dynamically recrystallized grain size as a palaeopiezometer in quartz-bearing mylonite zones. Tectonophysics 78, 475–508.

Ferguson, C.C., 1981. A strain reversal method for estimating extension from fragmented rigid inclusions. Tectonophysics 79, T43–T52.

Jamison, W.R., Spang, J.H., 1976. Use of calcite twin lamellae to infer differential stresses. Geological Society of America Bulletin 87, 868–872.

Ji, S., Zhao, P., 1993. Location of tensile fracture within rigid–brittle inclusions in a ductile flowing matrix. Tectonophysics 220, 23–31.

Ji, S., Saruwatari, K., 1998. A revised model for the relationship between joint spacing and layer thickness. Journal of Structural Geology 20, 1495–1508.

Ji, S., Zhu, Z., Wang, Z., 1998. Relationship between joint spacing and bed thickness in sedimentary rocks: effects of interbed slip. Geological Magazine 135, 637–655.

Lacombe, O., 2001. Paleostress magnitudes associated with development of mountain belts: insights from tectonic analyses of calcite twins in the Taiwan Foothills. Tectonics 20, 834–849.

Lloyd, G.E., Condliffe, E., 2003. 'Strain Reversal': a WindowsTM program to determine extensional strain from rigid–brittle layers or inclusions. Journal of Structural Geology 25, 1141–1145.

Lloyd, G.E., Ferguson, C.C., Reading, K., 1982. A stress-transfer model for the development of extension fracture boudinage. Journal of Structural Geology 4, 355–372.

Masuda, T., Kuriyama, M., 1988. Successive "mid-point" fracturing during microboudinage: an estimate of the stress–strain relation during a natural deformation. Tectonophysics 147, 171–177.

Masuda, T., Shibutani, T., Igarashi, T., Kuriyama, M., 1989. Microboudin structure of piedmontite in quartz schists: a proposal for a new indicator of relative palaeodifferential stress. Tectonophysics 163, 169–180.

Masuda, T., Shibutani, T., Kuriyama, M., Igarashi, T., 1990. Development of microboudinage: an estimate of changing differential stress with increasing strain. Tectonophysics 178, 379–387.

Masuda, T., Kugimiya, Y., Aoshima, I., Hara, Y., Ikei, H., 1999. A statistical approach to determination of a mineral lineation. Journal of Structural Geology 21, 467–472.

Masuda, T., Kimura, N., Hara, Y., 2003. Progress in microboudin method for palaeo-stress analysis of metamorphic tectonites: application of mathematically refined expression. Tectonophysics 364, 1–8.

Masuda, T., Kimura, N., Fu, B., Li, X., 2004. Validity of the microboudin method for palaeo-stress analysis: application to extraordinarily long sodic amphibole grains in a metachert from Aksu, China. Journal of Structural Geology 26, 203–206.

Mercier, J.-C.C., Anderson, D.A., Carter, N.L., 1977. Stress in the lithosphere: inferences from steady state flow of rocks. Pure and Applied Geophysics 115, 199–226.

Misch, P., 1969. Paracrystalline microboudinage of zoned grains and other criteria for synkinematic growth of metamorphic minerals. American Journal of Science 267, 43–63.

Okay, A.I., 2002. Jadeite–chloritoid–glaucophane–lawsonite blueschists in northwest Turkey: unusually high P/T ratios in continental crust. Journal of Metamorphic Geology 20, 757–768.

Okay, A.I., Harris, N.B.W., Kelley, S.P., 1998. Exhumation of blueschists along a Tethyan suture in northwest Turkey. Tectonophysics 285, 275–299.

Ord, A., Christie, J.M., 1984. Flow stresses from microstructures in mylonitic quartzites of the Moine Thrust Zone, Assynt area, Scotland. Journal of Structural Geology 6, 639–654.

Passchier, C.W., Trouw, R.A.J., 1996. Microtectonics. Springer, Berlin. 289pp.

Petry, M.D., Mah, T.-I., Kerans, R.J., 1997. Validity of using average diameter for determination of tensile strength and Weibull modulus of ceramic filaments. Journal of American Ceramic Society 80, 2741–2744.

Ramsay, J.G., 1967. Folding and Fracturing of Rocks. McGraw-Hill, New York. 568pp.

Rowe, K.J., Rutter, E.H., 1990. Paleostress estimation using calcite twinning: experimental calibration and application to nature. Journal of Structural Geology 12, 1–17.

Simmons, G., Wang, H., 1971. Single Crystal Elastic Constants and Calculated Aggregate Properties: A Handbook. MIT Press, Cambridge. 370pp.

Twiss, R.J., 1986. Variable sensitivity piezometric equations for dislocation density and subgrain diameter and their relevance to olivine and quartz. American Geophysical Union Geophysical Monograph 36, 247–261.

Weathers, M.S., Bird, J.M., Cooper, R.F., Kohlstedt, D.L., 1979. Differential stress determined from deformation-induced microstructures of the Moine Thrust Zone. Journal of Geophysical Research 84, 7495–7509.

Weibull, W., 1939. Statistical Theory of the Strength of Materials. Ingeniors Vetenskaps Akademi en Handlingar 151 (cited in Epstein, 1948).

Zhao, P., Ji, S., 1997. Refinements of shear-lag model and its applications. Tectonophysics 279, 37–53.